

Measurement of the Z/A dependence of neutrino charged-current total cross-sections

The CHORUS Collaboration

Abstract

A relative measurement of total cross-sections is reported for polyethylene, marble, iron, and lead targets for the inclusive charged-current reaction $\nu_\mu + N \rightarrow \mu^- + X$. The targets, passive blocks of ~ 100 kg each, were exposed simultaneously to the CERN SPS wide-band muon-neutrino beam over a period of 18 weeks. Systematic effects due to differences in the neutrino flux and detector efficiency for the different target locations were minimised by changing the position of the four targets on their support about every two weeks. The relative neutrino fluxes on the targets were monitored within the same experiment using charged-current interactions in the calorimeter positioned directly downstream of the four targets. From a fit to the Z/A dependence of the total cross-sections a value is deduced for the effective neutron-to-proton cross-section ratio.

To be published in The European Physical Journal C

The CHORUS Collaboration

A. Kayis-Topaksu, G. Onengüt
Çukurova University, Adana, Turkey

R. van Dantzig, M. de Jong, J. Konijn, O. Melzer, R.G.C. Oldeman¹, E. Pesen,
C.A.F.J. van der Poel, F.R. Spada², J.L. Visschers
NIKHEF, Amsterdam, The Netherlands

M. Güler³, M. Serin-Zeyrek, S. Kama, R. Sever, P. Tolun, M.T. Zeyrek
METU, Ankara, Turkey

N. Armenise, M.G. Catanesi, M. De Serio, M. Ieva, M.T. Muciaccia, E. Radicioni, S. Simone
Università di Bari and INFN, Bari, Italy

A. Bülte, K. Winter
Humboldt Universität, Berlin, Germany⁴

R. El-Aidi, B. Van de Vyver^{5,6}, P. Vilain⁷, G. Wilquet⁷
Inter-University Institute for High Energies (ULB-VUB) Brussels, Belgium

B. Saitta
Università di Cagliari and INFN, Cagliari, Italy

E. Di Capua
Università di Ferrara and INFN, Ferrara, Italy

S. Ogawa, H. Shibuya
Toho University, Funabashi, Japan

A. Artamonov⁸, J. Brunner⁹, M. Chizhov¹⁰, D. Cussans¹¹, M. Doucet¹², J.P. Fabre,
I.R. Hristova¹⁰, T. Kawamura, D. Kolev¹⁰, M. Litmaath¹³, H. Meinhard, J. Panman, I.M.
Papadopoulos, S. Ricciardi¹⁴, A. Rozanov⁹, D. Saltzberg¹⁵, R. Tsenov¹⁰, J.W.E. Uiterwijk,
P. Zucchelli¹⁶
CERN, Geneva, Switzerland

J. Goldberg
Technion, Haifa, Israel

M. Chikawa
Kinki University, Higashiosaka, Japan

E. Arik
Bogazici University, Istanbul, Turkey

J.S. Song, C.S. Yoon
Gyeongsang National University, Jinju, Korea

K. Kodama, N. Ushida
Aichi University of Education, Kariya, Japan

S. Aoki, T. Hara
Kobe University, Kobe, Japan

T. Delbar, D. Favart, G. Grégoire, S. Kalinin, I. Makhlyoueva
Université Catholique de Louvain, Louvain-la-Neuve, Belgium

P. Gorbunov⁶, V. Khovansky, V. Shamanov, I. Tsukerman
Institute for Theoretical and Experimental Physics, Moscow, Russian Federation

N. Bruski, D. Frekers, D. Rondeshagen, T. Wolff
Westfälische Wilhelms-Universität, Münster, Germany⁴

K. Hoshino, J. Kawada, M. Komatsu, M. Miyanishi, M. Nakamura, T. Nakano, K. Narita,
K. Niu, K. Niwa, N. Nonaka, O. Sato, T. Toshito
Nagoya University, Nagoya, Japan

S. Buontempo, A.G. Cocco, N. D'Ambrosio, G. De Lellis, G. De Rosa, F. Di Capua,
A. Ereditato, G. Fiorillo, A. Marotta, M. Messina, P. Migliozzi, C. Pistillo, R. Santorelli,

L. Scotto Lavina, P. Strolin, V. Tioukov

Università "Federico II" and INFN, Naples, Italy

K. Nakamura, T. Okusawa

Osaka City University, Osaka, Japan

U. Dore, P.F. Loverre, L. Ludovici, A. Maslennikov¹⁷, P. Righini, G. Rosa, R. Santacesaria,

A. Satta

Università La Sapienza and INFN, Rome, Italy

E. Barbuto, C. Bozza, G. Grella, G. Romano, C. Sirignano, S. Sorrentino

Università di Salerno and INFN, Salerno, Italy

Y. Sato, I. Tezuka

Utsunomiya University, Utsunomiya, Japan

¹ Now at University of Pennsylvania, Philadelphia, USA.

² And INFN, Rome, Italy

³ Now at Nagoya University, Nagoya, Japan.

⁴ Supported by the German Bundesministerium für Bildung und Forschung under contract numbers 05 6BU11P and 05 7MS12P.

⁵ Fonds voor Wetenschappelijk Onderzoek, Belgium.

⁶ Now at CERN, 1211 Geneva 23, Switzerland.

⁷ Fonds National de la Recherche Scientifique, Belgium.

⁸ On leave of absence from ITEP, Moscow.

⁹ Now at CPPM CNRS-IN2P3, Marseille, France.

¹⁰ St. Kliment Ohridski University of Sofia, Bulgaria.

¹¹ Now at University of Bristol, Bristol, UK.

¹² Now at University of Maryland, MD, USA.

¹³ Now at Fermi National Accelerator Laboratory, Batavia, IL, USA.

¹⁴ Now at Royal Holloway College, University of London, Egham, UK.

¹⁵ Now at U.C.L.A., Los Angeles, USA.

¹⁶ On leave of absence from INFN, Ferrara, Italy.

¹⁷ CASPUR, Rome, Italy.

1 Introduction

The charged-current (CC) interaction of muon-neutrinos (ν_μ) with nucleons $\nu_\mu + N \rightarrow \mu^- + X$ has been studied at accelerators for many years. The ν_μ CC total cross-section per nucleon has been found to rise linearly with the neutrino energy E_ν , and the coefficient of proportionality for an isoscalar target, $\sigma_T^{iso}(\nu N)/E_\nu$, is known today with 2% accuracy [1, 2, 3, 4]. In order to deduce $\sigma_T^{iso}(\nu N)/E_\nu$ from measurements on nuclei of atomic mass A , in general an appropriate correction needs to be applied to account for the non-isoscalarity of the target.

In previous experiments $\sigma(\nu n)$, $\sigma(\nu p)$ and $\sigma(\nu n)/\sigma(\nu p)$ have been measured. In bubble chamber experiments it was possible to distinguish neutrino interactions on neutrons and protons in deuterium [5, 6, 7] and in freon [8] targets. The absolute value of $\sigma(\nu p)$ was measured indirectly from interactions in hydrogen and a heavier target, neon [9] or iron [10]. All measurements are in good agreement with each other.

The CHORUS neutrino experiment (designed primarily for a neutrino oscillation search) collected data from spring 1994 to autumn 1998. The 1998 data-taking was entirely devoted to studies of cross-sections and structure functions [11]. Here we report on a part of this programme, namely relative measurements of the ν_μ CC total cross-sections for polyethylene, marble, iron and lead, using a new and straightforward measurement and analysis technique. These measurements of the cross-section ratios allow the Z/A -dependence of the total cross-section to be determined directly and, as a consequence, the effective neutron-to-proton cross-section ratio to be extracted. The results are compared with predictions obtained by a parametrisation of the quark densities in free nucleons [12, 13, 14].

The signature for the neutrino CC interaction $\nu_\mu + N \rightarrow \mu^- + X$ is a muon accompanied in most cases by a shower (X) of hadrons. Only the measurements of quantities related to the outgoing muon are required in this analysis. This method therefore eliminates systematic effects which would otherwise be introduced by the different target materials on the measurements of the hadronic final state. Quasi-elastic and resonance production are included in addition to the dominant deep-inelastic scattering (DIS) events.

2 Experimental set-up

A sketch of the experimental apparatus is shown in Fig. 1. Only part of the CHORUS detector is used, namely trigger hodoscopes, a tracking system made of honeycomb chambers, a calorimeter and a muon spectrometer. The other components of the CHORUS detector were not used in this measurement, but some of these remained in place. The data used in this analysis were acquired in 1998 when a set of four targets consisting of polyethylene, marble, iron and lead was added to the CHORUS detector. The apparatus was exposed to the wide-band neutrino beam produced by 450 GeV/ c protons from the CERN SPS. The average ν_μ energy is 27 GeV. The contamination of $\bar{\nu}_\mu$ is about 6% [15].

The four targets were positioned with their midplane perpendicular to the neutrino beam between the planes T and H of the trigger hodoscope (see Fig. 1). The targets were arranged in two columns and two rows, transversely separated by 20 cm air gaps. The blocks had the same transverse cross-section ($50 \times 50 \text{ cm}^2$) and approximately the same mass ($\sim 100 \text{ kg}$). In this way comparable statistics and a clear separation of the interactions from each target could be obtained. The properties of the target materials are summarised in Table 1.

The targets were placed on a light aluminium support. To minimise systematic effects due to variations in the neutrino flux and detector efficiency for the different target locations, the positions of the four targets on the support were changed about every two weeks.

The construction and performance of the various detectors are described in detail in Ref. [15] and we recall here only the points relevant for this analysis.

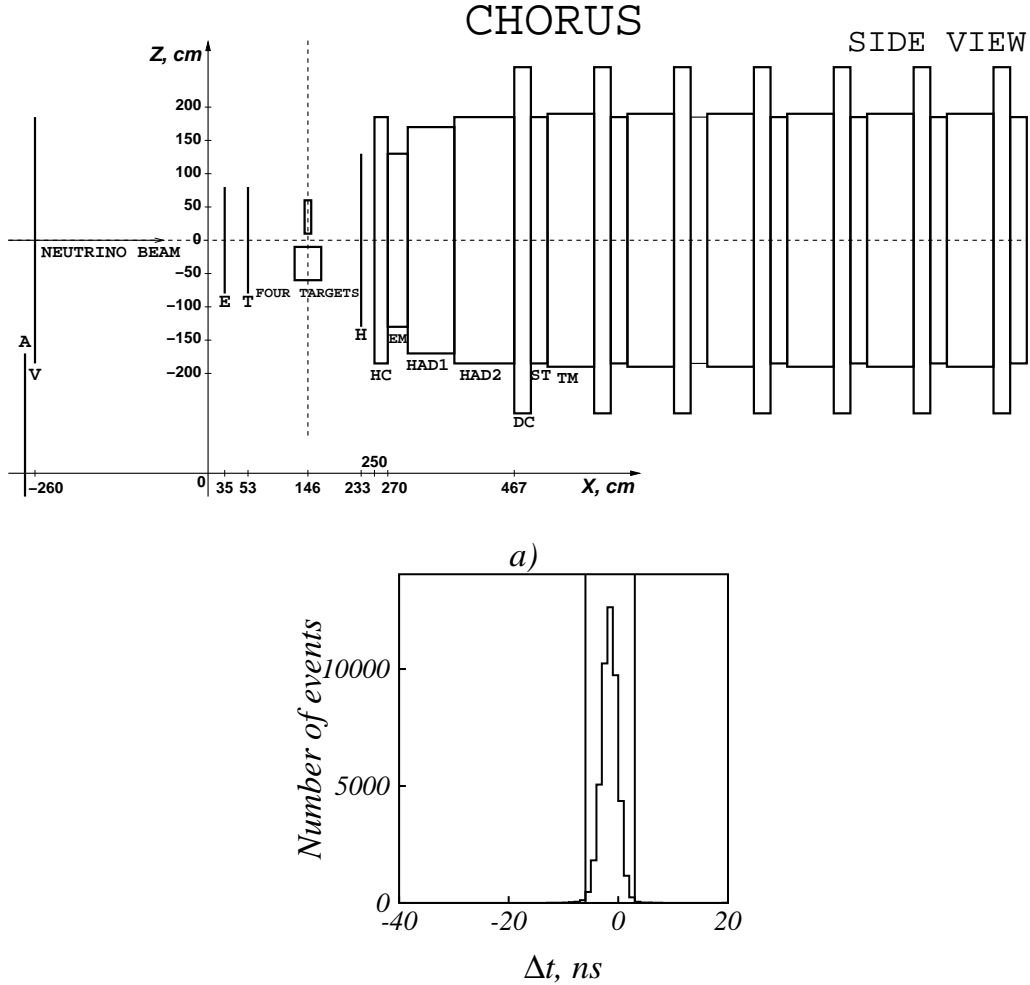


Figure 1: Side and front view of the configuration of the CHORUS detector and the four targets used for this exposure. The numbering of the target positions is indicated on the front view.

Just downstream of the targets and the H-hodoscope plane, the honeycomb tracker (HC) [16] provides tracking information. The tracker consists of three modules with wires oriented at 0° , 60° , and 120° with respect to the horizontal. Each module has six planes of drift tubes with hexagonal cross-section and a wire spacing of ~ 1 cm.

Further downstream, the lead-scintillator calorimeter [17] serves different purposes for this analysis: tracking of muons and recording of muon-neutrino CC interactions to calibrate the incoming neutrino flux at the four target locations. The calorimeter consists of fourteen planes of different thickness and granularity. Planes are perpendicular to the beam direction with scintillation strips oriented alternately horizontally and vertically. Eleven sets of streamer tubes are installed between the lead planes. Each set consists of one plane with vertical wires and one with horizontal wires.

The role of the muon spectrometer [15], situated downstream of the calorimeter, is to identify muons and to determine their trajectory, momentum, and charge. It consists of six toroidal iron magnets (TM), instrumented with scintillators, and tracking detectors composed of drift chambers (DC) and streamer tubes (ST). The systematic bias in the reconstructed momentum does not exceed 2.5% [11]. For muons within the acceptance the average momentum resolution is about 15–17% and the probability to misidentify the sign of the charge is below

Target	Material	Z	A g mol ⁻¹	X_0 g cm ⁻²	λ_0 g cm ⁻²	ρ g cm ⁻³	t cm	m kg	ρ_N 10 ²⁵ nucleons/cm ²
Plastic	(CH ₂) _n	5.29	9.28	44.6	78.4	0.935	42.5	98.6	2.38
Marble	CaCO ₃	12.56	25.16	24.01	106.49	2.75	15	100.7	2.43
Iron	Fe	26	55.85	13.84	131.9	7.87	5	99.3	2.39
Lead	Pb	82	207.2	6.37	194.0	11.35	4	113.5	2.73

Table 1: Properties of the materials used as targets in the present experiment: radiation length (X_0), interaction length (λ_0), mass density (ρ), target thickness (t), mass (m) and the number of nucleons/cm², $\rho_N = mN_A/S$, with N_A the Avogadro number and S the surface of the targets.

0.2%.

Five planes of scintillator hodoscopes (labelled A, V, E, T, H) were used for on-line triggering and analysis purposes. The configuration of these hodoscopes is shown in Fig. 1 and a detailed description of their design and performance is given in Ref. [18]. Only those properties which are essential for an understanding of this analysis will be mentioned here. The T-hodoscope system was made of two staggered planes of scintillator strips, coupled at both ends to a photomultiplier and oriented horizontally. It was located 93 cm upstream of the midplane of the four targets. The H-hodoscope system consisted of two staggered planes with photomultipliers at one end only. The photomultipliers of the second plane were coupled at the opposite end to those of the first plane. The H-hodoscope system was positioned in front of the honeycomb tracker, 87 cm downstream of the four targets. The pulse height of the photomultiplier signals was measured by ADCs and in addition a bit was stored for each signal exceeding the discriminator threshold. The time difference between a T- and an H-hit was used to provide a separation between forward going particles (e.g. muons created in the material upstream of the targets) and backward going particles. To acquire timing information TDCs with 64 μ s dynamic range and a resolution of 1 ns were used. A high-intensity 100 GeV/ c muon beam was used for precise “time-zero” calibration at the beginning of the data collection period.

3 Event selection

The on-line trigger system selects interactions in the four targets and in the calorimeter simultaneously. The trigger logic required signals consistent with a track in the calorimeter and the spectrometer, as well as the absence of activity in the V- and A-planes which therefore vetoes beam-related muons. A *fiducial volume* condition is satisfied if three or more of calorimeter planes seven to twelve are hit in their central parts. In addition, at least one plane of each orientation should have a hit. A *penetration* condition requires signals in at least two magnets of the muon spectrometer. In special timing and calibration runs the V-plane is used as a requirement in the trigger to select beam muons.

The data are recorded in periods which differ according to the configuration of the group of targets. The number of protons on target corresponding to this period of data-taking is 0.54×10^{19} roughly equally distributed among the configurations. A two-day period with the target blocks removed (*empty-target* period) was taken to evaluate and subtract the background due to neutrino interactions in the materials surrounding the targets.

The event reconstruction starts in the spectrometer, in an environment with relatively low track density. Information from the drift chambers and the streamer tubes is used to form muon track candidates. The tracking algorithm (see for example Ref. [19]) takes into account the magnetic field as well as the energy loss and multiple Coulomb scattering, and yields the momentum and direction of muons at the upstream face of the spectrometer. Initial track param-

Configuration	1	2	3	4	empty-target
Events	1, 273, 145	590, 840	1, 034, 232	963, 686	102, 093
POT, 10^{13}	178, 499	83, 130	144, 533	134, 420	16, 384
<i>Four-target sample</i>					
Events	261, 787	120, 930	212, 745	199, 644	19, 818
Negatively charged muon	248, 895	114, 908	202, 559	189, 812	18, 809
$p_\mu \geq 4 \text{ GeV}/c$	222, 328	102, 717	181, 242	169, 937	16, 766
HC hits > 7	65, 009	30, 102	53, 694	51, 387	4, 146
T geometry	35, 600	16, 595	29, 779	28, 672	1, 838
T and H TDCs	22, 290	10, 302	18, 102	17, 096	835
Four-target geometry	18, 188	8, 501	14, 816	13, 936	546
Position 1	4, 297 (marble)	2, 147 (iron)	4, 130 (lead)	3, 239 (plastic)	135 (empty)
Position 2	4, 262 (plastic)	1, 953 (marble)	3, 375 (iron)	3, 574 (lead)	133 (empty)
Position 3	4, 436 (iron)	2, 372 (lead)	3, 635 (plastic)	3, 589 (marble)	149 (empty)
Position 4	5, 193 (lead)	2, 029 (plastic)	3, 676 (marble)	3, 534 (iron)	129 (empty)
<i>Calorimeter sample</i>					
Events	1, 011, 358	469, 910	821, 487	764, 042	82, 275
Negatively charged muon	952, 159	442, 421	773, 500	719, 843	77, 668
$p_\mu \geq 4 \text{ GeV}$	845, 000	392, 427	686, 786	639, 502	68, 848
HC hits = 0	820, 640	381, 006	666, 262	619, 923	66, 932
Four-target geometry	278, 781	129, 745	227, 263	212, 313	22, 745
Position 1	66, 649	31, 568	55, 444	52, 051	5, 555
Position 2	67, 772	31, 396	54, 416	50, 933	5, 541
Position 3	71, 426	33, 673	58, 938	54, 931	5, 808
Position 4	72, 934	33, 108	58, 465	54, 398	5, 841

Table 2: Number of events with a reconstructed muon in the spectrometer for the five configurations and four positions are listed after applying each selection cut. The separation of the four-target sample and the calorimeter sample is based on the activity recorded in the H-plane.

eters with their error matrices are propagated from the spectrometer in the upstream direction using the streamer-tube planes of the calorimeter and the drift-tube planes of the honeycomb tracker. Straight line extrapolations from the downstream detectors are used to determine impact parameters of the muon at the H and T counters and the four-target midplane. In total about 4.0×10^6 muon tracks are reconstructed and extrapolated to the four-target midplane. If more than one muon track is found in the spectrometer, the one with the highest momentum is taken.

After reconstruction of the muon track, the information of the H-plane is used to separate events with their origin in the targets from those originating in the calorimeter, referred to as the *four-target* and the *calorimeter sample*, respectively. Muons generated in the calorimeter are used for the relative normalisation of the different four-target subsamples.

The accumulated statistics in the two distinct samples is given in Table 2. Events are first divided into five groups according to the target configuration periods. For each of the periods, the four-target sample is selected by requiring at least one hit in at least one of the two H trigger counters.

The following additional cuts are applied to the two samples. Interactions by incident neutrinos are selected by requiring muons with negative charge. To reject punch-through hadrons in the muon spectrometer as well as secondary muons from hadron decay, and to ensure correct charge determination and high reconstruction efficiency, the muon momentum at the entrance of the spectrometer is required to be larger than $4 \text{ GeV}/c$ (this implies an effective cut of $\approx 6 \text{ GeV}/c$ at the interaction vertex since muons have to traverse the calorimeter before being

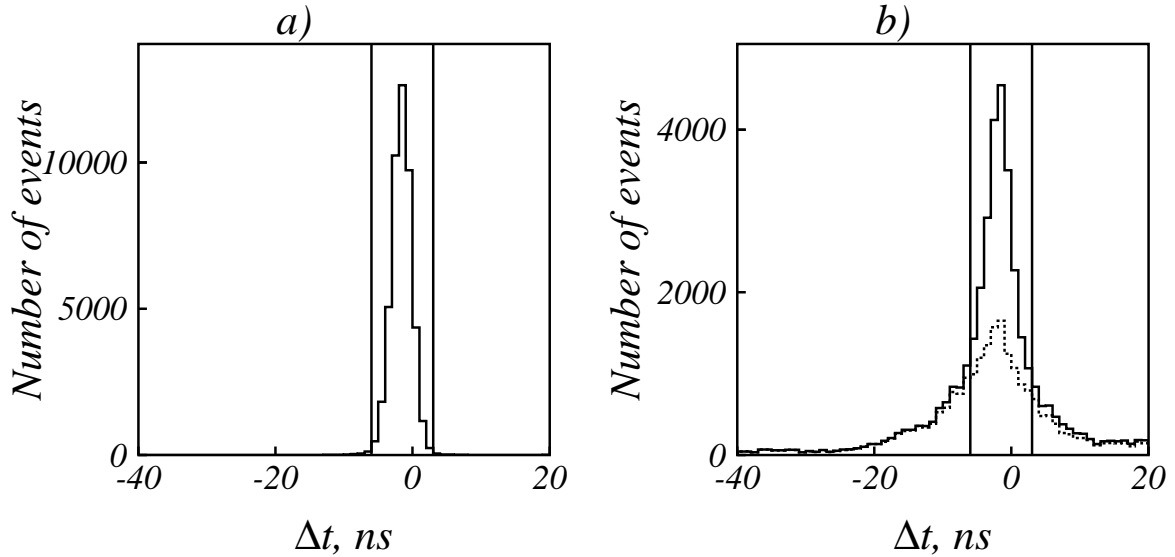


Figure 2: TDC spectra of the time difference between the T- and H-hits nearest to the muon track: a) for incoming muons selected by requiring a hit in the V-plane; b) for the four-target sample before timing cuts are applied (solid histogram), and for the four-target sample after the rejection of traversing muons using the time difference of the hits on the muon track within a 3σ road (dashed histogram). (The time window used for the rejection is indicated with vertical lines; the entries remaining inside this time window represent hits outside the 3σ road.)

measured in the spectrometer). It was checked with a simulation that the difference in energy loss in the different materials of the four targets has a negligible effect (less than 0.1% of the events) on this selection.

From the calorimeter sample, events with no hits along the track in the HC-planes are selected for the normalisation. This requirement ensures that the muon is not produced in one of the targets. Events with their origin in the calorimeter and a backward going charged particle would still be erroneously assigned to the four-target sample. Requiring more than seven hits along the muon track in the honeycomb tracker, with at least three hits in at least two modules, allows optimal separation of four-target events from calorimeter events with backscattering. Any remaining background contribution from the calorimeter is subtracted implicitly using the empty-target data.

To be accepted as a candidate with its origin in the four targets, a muon must extrapolate to the sensitive area of the T-plane within a region which is 10 cm wider than the actual target area. The effect of this selection is shown on the line labelled “T geometry” in Table 2.

An event is rejected if there is a hit located within a 3σ road around the muon impact points at the T-plane and the H-plane and if the time difference between the two hits is consistent with a relativistic particle crossing the four-target set-up (Fig. 2). This strongly suppresses the main peak due to muons traversing the four-target set-up, while most of the T-H coincidences due to backscattering from the four targets are preserved in the much lower and broader peak that remains.

Four squares of 53 cm sides are defined at the midplane of the target set-up, each corresponding to one target position (see Fig. 1). Events belonging to the four-target sample are assigned to a specific target on the basis of their predicted geometrical impact point at this plane. Similarly, for the calorimeter sample events are assigned to normalisation samples correspond-

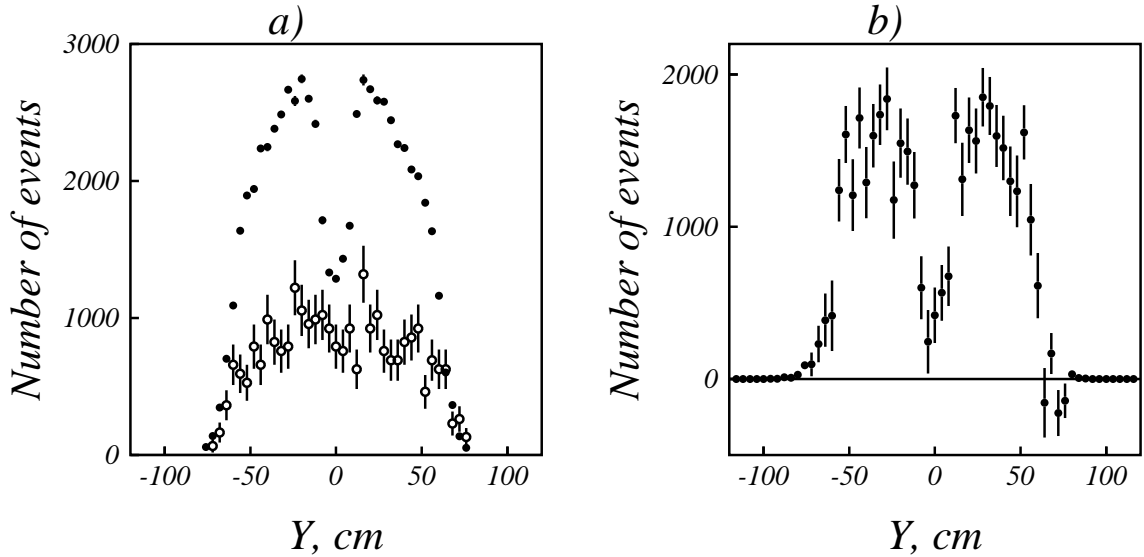


Figure 3: The horizontal projections for the four-target sample a) solid circles: four-target sample including background events; open circles: the normalised empty-target background sample; b) with the normalised empty-target background subtracted. The distributions in the vertical projections are similar.

Target	$\sigma^A(\nu N)/C$ $10^{-27}\text{cm}^2/\text{nucleon}$	$\sigma^A(\nu N)/\sigma^{\text{marble}}(\nu N)$
Polyethylene	$6.39 \pm 0.10_{\text{stat}} \pm 0.17_{\text{subtr}} \pm 0.19_{\text{syst}}$	$0.977 \pm 0.021_{\text{stat}} \pm 0.006_{\text{syst}}$
Marble	$6.54 \pm 0.10_{\text{stat}} \pm 0.17_{\text{subtr}} \pm 0.18_{\text{syst}}$	
Iron	$6.74 \pm 0.10_{\text{stat}} \pm 0.17_{\text{subtr}} \pm 0.21_{\text{syst}}$	$1.031 \pm 0.022_{\text{stat}} \pm 0.007_{\text{syst}}$
Lead	$6.97 \pm 0.08_{\text{stat}} \pm 0.15_{\text{subtr}} \pm 0.20_{\text{syst}}$	$1.066 \pm 0.022_{\text{stat}} \pm 0.008_{\text{syst}}$

Table 3: Cross-section results $\sigma^A(\nu N)/C$, where C is a normalisation constant. For ease of comparison with other experiments the ratio of cross-sections relative to marble, which is isoscalar, is given in the third column. The component of the uncertainty labeled *subtr* indicates the statistical error introduced by the background subtraction. The correlation introduced by the subtraction is taken into account in the statistical error of the ratios in column three.

ing to the four different targets again on the basis of their geometrical location. The neutrino flux is therefore monitored by the CC event rate in the calorimeter for each target position separately. The normalisation of the empty-target sample is also based on the corresponding events in the calorimeter. The distribution of the impact points is shown in Fig. 3, which demonstrates the geometrical separation of events.

4 Results and discussion

Experimentally, the neutrino CC total cross-section per nucleon may be written as $\sigma^A(\nu N) = N^\mu / (\Phi^\nu \rho_N)$, where N^μ is the number of muons produced in the target, Φ^ν is the number of incident neutrinos integrated over the energy spectrum and area, and ρ_N the thickness of the target in nucleons per cm^2 . The integrated neutrino flux Φ^ν is not measured in this experiment, therefore it is not possible to obtain absolute cross-sections. Furthermore, relative knowledge of the neutrino flux is needed when taking the ratio $\sigma^{A_i}(\nu N)/\sigma^{A_j}(\nu N)$ for a given pair of targets A_i and A_j , since the neutrino fluxes collected during the periods with different configuration

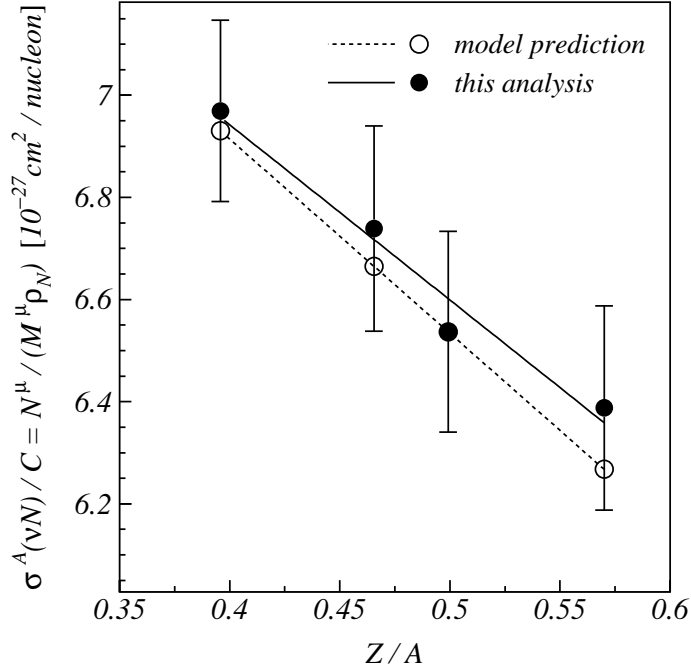


Figure 4: The measurements of the relative total cross-sections, $\sigma^A(\nu N)/C$, plotted as a function of Z/A (filled dots). The predictions of the cross-section model described in the text are superimposed (open dots) such that the measured and the model points for marble coincide on the plot. The solid and the dashed lines represent the best linear fits to the data and the model points calculated for the acceptance of this experiment, respectively.

were not identical.

This information can be obtained from the number of muons, M^μ , in the calorimeter sample. The flux is then expressed as $\Phi^\nu = M^\mu / (\sigma^{calo}(\nu N) \rho_N^{calo})$, where the denominator is a constant, C , equal for all four targets. The ratios (N^μ/M^μ) for all four target materials thus measure the cross-sections up to a common constant. From the measured event rates in the targets and the calorimeter for each target position is computed

$$\left(\frac{N^\mu}{M^\mu}\right)_j = \sum_{i=1}^4 \left(\frac{N_{ij}}{M_{ij}} - \frac{N_{i0}}{M_{i0}}\right) \equiv \sum_{i=1}^4 \left(\frac{N_{ij}}{M_{ij}}\right) - E, \quad (1)$$

where the index $i = 1, 2, 3, 4$ runs over the four possible positions, and j gives the target material (polyethylene, marble, iron or lead); $j = 0$ refers to the empty-target configuration, and where $E = \sum_{i=1}^4 \left(\frac{N_{i0}}{M_{i0}}\right)$.

The results for $\sigma^A(\nu N)/C$ are given in Table 3 and plotted as a function of Z/A in Fig. 4. Both statistical and systematic errors are quoted in Table 3. The correlated statistical error introduced by the empty-target background subtraction is given separately from the statistical error on the target counts. Also given in Table 3, for ease of comparison with other experiments, is the ratio of cross-sections relative to marble, which is isoscalar. The individual sources of systematic uncertainty are given in Table 4. The two statistical errors are summed quadratically

Cuts	Shift	Syst. error $\times 10^3$			Syst. error on $\sigma(\nu n)/\sigma(\nu p)$
		$\sigma^{plastic}/\sigma^{marble}$	$\sigma^{iron}/\sigma^{marble}$	$\sigma^{lead}/\sigma^{marble}$	
p_μ	± 1 GeV	4.3	3.9	2.4	0.031
Four-target geometry	± 1 cm	2.3	4.1	6.8	0.047
Calorimeter geometry	± 1 cm	1.0	0.6	0.5	0.015
HC hits required	± 1 hit	1.7	0.4	0.8	0.025
T-plane geometry	± 1 cm	1.6	0.9	1.7	0.002
TDC cut (lower limit)	± 1 ns	1.5	0.8	1.4	0.006
TDC cut (higher limit)	± 1 ns	0.5	0.5	0.5	0.006
Target mass uncertainty	$\pm 0.2\%$	2.7	2.9	3.0	0.048
Total		6.3	6.5	8.1	0.080

Table 4: Sources of systematic errors and their contribution to the error of the cross-section ratios and the neutron-to-proton cross-section ratio. The total systematic error is obtained by adding the components in quadrature.

and plotted in Fig. 4 for each target. The measurement of the Z/A -dependence is a direct experimental result and thus it is independent of models describing neutrino-nucleus cross-sections.

These experimental results can be interpreted in terms of an *effective* cross-section ratio $\sigma(\nu n)/\sigma(\nu p)$ sampled with the acceptance of the present detector exposed to the CERN neutrino beam. To obtain $\sigma(\nu n)/\sigma(\nu p)$ it is assumed that the neutrino-nucleus total cross-section is an incoherent weighted sum of the neutron and proton cross-sections. The cross-section per nucleon is then a linear function of Z/A with two parameters: $\sigma(\nu A)/A = (Z/A)p_1 + p_2$, where $p_1 = \sigma(\nu p) - \sigma(\nu n)$ and $p_2 = \sigma(\nu n)$.

The solid line in Fig. 4 represents the best linear fit to the four data points, from which the value

$$\frac{\sigma(\nu n)}{\sigma(\nu p)} = 1.71 \pm 0.22_{stat} \pm 0.08_{syst} \quad (2)$$

for the effective neutron-to-proton cross-section ratio is obtained. Systematic errors have been evaluated by repeating the same analysis with variations on the selections reflecting the uncertainties. Contributions to the uncertainties in the relative cross-section measurements and the $\sigma(\nu n)/\sigma(\nu p)$ uncertainty are listed in Table 4.

A parton model calculation was performed using a set of quark distribution functions (GRV98LO [12]) available from PDFLIB [13] and modified according to the model described in [14]. This model uses a new improved scaling variable and adds modifications in order to describe cross-sections at both very low and high energies. Quasi-elastic scattering, resonance production, longitudinal structure function, radiative corrections ([20]) and nuclear effects are taken into account in the calculations. The model calculation predicts for the neutron-to-proton cross-section ratio a value of 1.87 for our energy spectrum and for a detector with full acceptance.

Within the uncertainties the present result for $\sigma(\nu n)/\sigma(\nu p)$ is in agreement with the results of previous neutrino experiments [5, 6, 7, 8, 9, 10] as shown in Table 5. Small differences between the experiments may be understood by their different energy spectra and kinematic acceptances. The largest effect arises from the x -dependence of $\sigma(\nu n)/\sigma(\nu p)$, which in turn translates into a dependence on θ_μ . As an illustration, we obtain a value of 1.82 using the model described above with the angular acceptance for this experiment. The predictions of the quark model are plotted as a function of Z/A (open dots) in Fig. 4 for the acceptance of this experiment. They are scaled so that the model prediction coincides with the measured point for

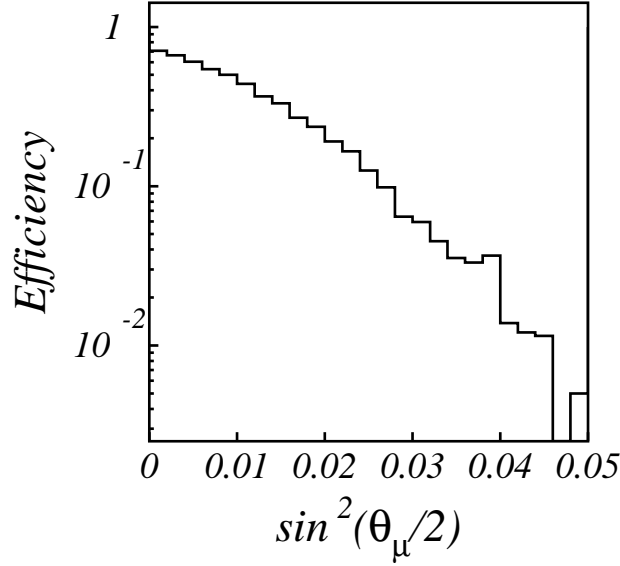


Figure 5: Dependence of the acceptance on $\sin^2(\theta_\mu/2)$, where θ_μ is the angle of the muon.

marble. For ease of comparison of the data with other models the acceptance is shown in Fig. 5. The effective cut of 6 GeV/ c applied on the muon momentum has a negligible effect on the predicted ratio.

Although some of the errors of the experiments quoted in Table 5 appear to be smaller, they are of different nature than the ones in the measurement presented here. In the bubble chamber experiments with a single liquid [5, 6, 7, 8], the events had to be separated as an interaction on a neutron to a proton on the basis of the event topology. The systematic errors quoted in the deuterium events [5, 6, 7] are therefore correlated, while in a heavier liquid (CF₃Br [8]) one would expect a larger uncertainty. It should also be noted that the average neutrino energy in the SKAT experiment is 7 GeV, much lower than the average energy of the beam used in this experiment which is similar to the beam used for the other experiments quoted. The experiments where a hydrogen target is compared with a nuclear target [9, 10] have other uncertainties since the interactions from the two different targets cannot be treated in an identical way. The result of the CDHS experiment is not directly quoted in their paper, but was derived indirectly by us.

A calculation using a model for nuclear effects [13, 21] predicts a change of $\sigma(\nu n)/\sigma(\nu p)$ by less than 1%. Nuclear corrections to the quasi-elastic and resonance production cross-section [22] increase the estimate of $\sigma(\nu n)/\sigma(\nu p)$ by less than 5%. Therefore, measurement errors do not allow us to draw definite conclusions about possible nuclear and other effects which might affect the cross-sections on neutrons and protons.

5 Summary and conclusions

Relative measurements of muon-neutrino charged-current (CC) total cross-sections for several nuclear targets were performed for the first time within the same experiment. Due measures have been taken during the running and analysis stages of the experiment to minimise the effect of systematic errors on the results of this measurement:

- events were assigned as originating from the different targets on the basis of geometrical criteria;
- only muons were used in the event reconstruction;
- the targets were exposed simultaneously to the neutrino beam;

Experiment	Year	Target(s)	ν_μ CC events	$R^\nu \equiv \sigma(\nu n)/\sigma(\nu p)$	$\Delta R^\nu/R^\nu$
BEBC [5]	1981	D ₂	1.4k	$2.22 \pm 0.12 \pm 0.25$	13%
BEBC [6]	1984	D ₂	7.0k	$2.10 \pm 0.08 \pm 0.22$	11%
15-ft FNAL [7]	1980	D ₂	3.9k	$2.03 \pm 0.08 \pm 0.27$	14%
SKAT [8]	1989	CF ₃ Br	4.3k	$2.24 \pm 0.18 \pm 0.07$	8%
BEBC-TST [9]	1984	H/Ne	1.9k	$1.98 \pm 0.18 \pm 0.05$	10%
CDHS [10]	1984	H/Fe	57k	2.07 ± 0.14	7%
this analysis (CHORUS)	2002	(CH ₂) _n /CaCO ₃ /Fe/Pb	37k	$1.71 \pm 0.22 \pm 0.08$	13%

Table 5: Results for the neutron-to-proton cross-section ratio from previous neutrino experiments together with our result. The result of the CDHS experiment is not directly quoted in their paper, but was derived indirectly by us.

- the targets were rotated among the four positions to avoid differences in acceptance;
- an empty-target period was recorded and used for background subtraction;
- neutrino CC interactions in the calorimeter were taken simultaneously with the four-target data and used for internal monitoring of the neutrino flux and for relative normalisation of the events in the four targets.

Owing to the experimental method used, the cross-sections on the different materials have been measured completely symmetrically. It should be stressed that the separation of events according to their origin in the different materials was based on purely geometrical criteria. Therefore, the results do not depend on model-dependent corrections which may introduce unknown systematic errors.

The relative CC total cross-sections per nucleon on polyethylene, marble, iron, and lead targets were measured and the Z/A dependence found to be in agreement with predictions obtained with a parton model calculation using a parametrisation of quark densities in free nucleons. The neutron-to-proton cross-section ratio was deduced from a fit to the Z/A dependence of the measured relative CC total cross-sections for the four target materials. The result is in agreement with the data from previous experiments within the measurement uncertainties. It also agrees with predictions obtained by the parton model calculation mentioned above.

Acknowledgements

We gratefully acknowledge the help and support of the neutrino-beam staff and of the numerous technical collaborators who contributed to the detector construction and operation. The experiment has been made possible by grants from the Institut Interuniversitaire des Sciences Nucléaires and the Interuniversitair Instituut voor Kernwetenschappen (Belgium); the Israel Science Foundation (grant 328/94) and the Technion Vice President Fund for the Promotion of Research (Israel); CERN (Geneva, Switzerland); the German Bundesministerium für Bildung und Forschung (Germany); the Institute of Theoretical and Experimental Physics (Moscow, Russia); the Istituto Nazionale di Fisica Nucleare (Italy); the Promotion and Mutual Aid Corporation for Private Schools of Japan and Japan Society for the Promotion of Science (Japan); the Korea Research Foundation Grant (KRF-2001-005-D00006) (Republic of Korea); the Foundation for Fundamental Research on Matter FOM and the National Scientific Research Organisation NWO (The Netherlands); and the Scientific and Technical Research Council of Turkey (Turkey). We gratefully acknowledge their support.

We would like to thank Prof. E. Paschos and Dr. J.Y. Yu for fruitful discussions.

References

- [1] K. Hagiwara *et al.*, Phys. Rev. **D66** (2002) 010001, 261.
- [2] P. Berge *et al.*, CDHSW Collaboration, Z. Phys. **C35** (1987) 443.
- [3] P.S. Auchincloss *et al.*, CCFR Collaboration, Z. Phys. **C48** (1990) 411.
- [4] J.V. Allaby *et al.*, CHARM Collaboration, Z. Phys. **C38** (1988) 403.
- [5] D. Allasia *et al.*, Phys. Lett. **B107** (1981) 148.
- [6] D. Allasia *et al.*, Nucl. Phys. **B239** (1984) 301.
- [7] C.Y. Chang *et al.*, Phys. Rev. Lett. **45** (1980) 1817.
- [8] J. Brunner *et al.*, Z. Phys. **C42** (1989) 361.
- [9] N. Armenise *et al.*, Phys. Lett. **B102** (1981) 374.
- [10] H. Abramowicz *et al.*, Z. Phys. **C25** (1984) 29.
- [11] R.G.C. Oldeman, PhD thesis, University of Amsterdam, June 2000, <http://choruswww.cern.ch/Reference/Theses/Theses.html>.
- [12] M. Glück, E. Reya and A. Vogt, Eur. Phys. J. **C5** (1998) 461.
- [13] H. Plothow-Besch, J. Mod. Phys. **A10** (1995) 2901; H. Plothow-Besch, Users' Manual-Version 8.04, W5051 PDFLIB, 2000.04.17, CERN-PPE.
- [14] A Bodek and U.K. Yang, to appear in the proceedings of 4th NuFact '02 Workshop (Neutrino Factories based on Muon Storage Rings), London, England, 1-6 Jul 2002, submitted to J. Phys. G, hep-ex/0210024; A. Bodek and U.K. Yang, presented at 1st Workshop on Neutrino–Nucleus Interactions in the few GeV Region (NuInt01), Tsukuba, Japan, 13-16 Dec 2001, Nucl. Phys. Proc. Suppl. 112:70-76,2002, hep-ex/0203009.
- [15] E. Eskut *et al.*, CHORUS Collaboration, Nucl. Instrum. Methods **A401** (1997) 7.
- [16] J.W.E. Uiterwijk *et al.*, CHORUS Collaboration, Nucl. Instrum. Methods **A409** (1998) 682.
- [17] S. Buontempo *et al.*, CHORUS Collaboration, Nucl. Instrum. Methods **A349** (1994) 70.
E. Di Capua *et al.*, CHORUS Collaboration, Nucl. Instrum. Methods **A378** (1996) 221.
- [18] M.G. van Beuzekom *et al.*, CHORUS Collaboration, Nucl. Instrum. Methods **A427** (1999) 587.
- [19] M. Holder *et al.*, CDHS Collaboration, Nucl. Instrum. Methods **148** (1978) 235.
- [20] D. Yu. Bardin and V. A. Dokuchaeva, JINR-E2-86-260; the tables were updated using recent structure functions [12].
- [21] K.J. Eskola, V.J. Kolhinen and C.A. Salgado, Eur. Phys. J. **C9** (1999) 61.
- [22] E.A. Paschos and J.Y. Yu, Phys. Rev. **D65** (2002) 033002; E.A. Paschos *et al.*, Nucl. Phys. **B588** (2000) 263.